

# Microstrain and self-limited grain growth in nanocrystalline ceria ceramics

Jennifer L.M. Rupp \*, Anna Infortuna, Ludwig J. Gauckler

*Nonmetallic Inorganic Materials, Department of Materials, Swiss Federal Institute of Technology, ETH Zurich, Wolfgang-Pauli-Street 10, CH-8093 Zurich, Switzerland*

Received 8 February 2005; received in revised form 21 November 2005; accepted 22 November 2005  
Available online 21 February 2006

## Abstract

The grain coarsening in dense nanocrystalline gadolinia-doped ceria (CGO) and CeO<sub>2</sub> was studied for the grain size regime from 10 to 250 nm. Dense ceria-based thin films were prepared by spray pyrolysis and pulsed laser deposition on sapphire substrates. The small grain-sized CGO and CeO<sub>2</sub> microstructures were surprisingly stable and showed self-limited grain growth and relaxation of the microstrain with time. In this regime, material transport occurs via grain boundary diffusion leading to densification and grain coarsening in the thin films. A continuous transition to common grain growth kinetics was observed for larger grains at higher temperatures. © 2005 Acta Materialia Inc. Published by Elsevier Ltd. All rights reserved.

*Keywords:* Grain growth; Ceramics; Microstrain; Ceria; Thin films

## 1. Introduction

In the last years, gadolinia-doped ceria (CGO) electrolytes have drawn much attention as electrolytes for solid oxide fuel cells (SOFC) operating at intermediate temperatures due to their high-ionic conductivity compared to state-of-the-art yttria stabilized zirconia (YSZ) electrolytes [1–4]. The use of thin film electrolytes minimizes the ohmic loss across the electrolyte and SOFC operation at lower temperatures is possible as the power output is increased [5,6]. YSZ is used in micro solid oxide fuel cells ( $\mu$ -SOFC) in the form of thin film electrolytes with thicknesses of some hundred nanometer [7]. In an earlier paper Gödickemeier and Gauckler [8] highlighted the conditions when the mixed conducting ceria can be used as electrolytes in SOFC avoiding short circuiting through its electronic conductivity. In prior SOFC-related work, ceria thin films were deposited by physical vapor deposition (PVD) [9], chemical vapor deposition (CVD) [10], spin coating [11] and spray pyrolysis [5,12]. The latter technique offers the

possibility to produce dense thin films in the amorphous state. These films can then be crystallized without the development of columnar grains by heat treatment. Pulsed laser deposition results in thin films with an average grain size of roughly  $\sim 15$  nm after deposition. Both methods allow the preparation of dense material and grain growth kinetics can be studied.

Recently grain growth kinetics were reported for ceria with a grain size in the micron and submicron regime [13]. Indications for self-limited grain growth were shown in ceria with a grain size of 50–250 nm. Whereas the coarser grained material obeyed the classical parabolic grain growth law, the fine microstructures attained a limited grain size after a short dwell at low temperature.

The objective of this study is to investigate the grain growth of nanocrystalline CGO solid solutions at the potential operating conditions of  $\mu$ -SOFCs and gas separation membranes, e.g., 500–800 °C. The results will elucidate whether the grain growth kinetics that prevail differ from those associated with the classical view of grain-boundary-controlled migration kinetics, and whether CGO thin films develop microstructures that are sufficiently stable to allow extended use in  $\mu$ -SOFC devices.

\* Corresponding author. Tel.: +41 1 632 5651; fax: +41 1 632 11 32.  
E-mail address: [jennifer.rupp@mat.ethz.ch](mailto:jennifer.rupp@mat.ethz.ch) (J.L.M. Rupp).

## 2. Grain growth kinetics

More than 50 years ago, Burke and Turnbull deduced the kinetics of isothermal grain growth from the movement of grain boundaries for polycrystalline materials [14,15]. The authors assume that the driving force for grain boundary migration results from the grain face intersections at nonequilibrium angles and from the strong curvatures at grain faces. Both effects are connected, since if grain intersections approach equilibrium angles, strong grain curvature would be introduced, or, if the grain faces were mechanically straightened interfacial angles would change. In this sense, grain growth can be described as a curvature induced process, where atoms diffuse across and along the grain boundaries and the specific grain boundary area is reduced. [14]. In Burke's and Turnbull's formulation of the parabolic grain growth the grain growth rate  $\frac{dG}{dt}$  is related to the mean radius of grain curvature, which is proportional to the average grain size  $G$  [15].

$$\frac{dG}{dt} = \frac{M\gamma}{G} \quad (1)$$

Here, the proportionality constant is the product of the grain boundary energy  $\gamma$  and the grain boundary mobility  $M$ . The solution of Eq. (1) leads to:

$$G^2 - G_0^2 = k_2 t \quad (2)$$

where  $k_2 = 2M\gamma$  is a characteristic material constant. However, in many of the grain growth experiments a non parabolic grain growth behavior is observed [16]. This is given by [17]:

$$G^n - G_0^n = k_n t \quad (3)$$

with the material constant

$$k_n = nM\gamma G^{n-2} \quad (4)$$

Eqs. (3) and (4) reduce to the special case of the parabolic grain growth law (Eq. (2)) for a grain growth exponent  $n = 2$ . Experimentally grain growth exponents between  $n = 2$  and  $n = 4$ , but in some cases even up to  $n = 10$  were reported [18–22]. Many reasons were put forward to explain deviations from the theoretically expected parabolic law, e.g., that impurities or pores affect the grain growth kinetics. Grain growth exponents also depend on temperature within a given polycrystalline system [13]. In many cases these relations are still insufficient to describe grain growth, especially when the grain sizes are small, e.g., in the nanometer regime. Recently grain growth data from microcrystalline metals were described by the generalized grain growth model (Eq. (3)), whereas the grains in nanocrystalline metals grew until a certain limited grain size was reached, upon which grain growth ceased [23–25]. It was shown that the limited grain boundary migration was due to the grain size dependent solute drag of nanocrystalline metals. In addition to being impeded by solute drag, grain growth can also be impeded by defects in the material. Nanocrystalline sputtered gold thin films showed

limited grain growth being strongly affected by the amount of defects present [26]. During isothermal annealing the grains grew as long as the microstrain decreased. Once the microstrain relaxed in the thin films the grain growth ceased and metastable microstructures developed. In studies on the crystallization of amorphous Zr–Ti(Nb)–Cu–Ni–Be(Al) alloys it was confirmed that nucleation and crystal growth occur simultaneously until a metastable equilibrium is reached where grain growth stops [27,28]. With increasing temperatures a transition to classical parabolic grain growth law was observed.

The aim of this study is to investigate the grain growth and microstrain evolution in nanocrystalline ceramics of undoped and gadolinia-doped ceria thin films for the grain size range from 10 to 250 nm. In the present study we used dense films where the film thickness was always kept larger than the average grain size.

## 3. Experimental procedures

### 3.1. Thin film preparation and characterization

Undoped ceria ( $\text{CeO}_2$ ) and gadolinia-doped ceria,  $\text{Ce}_{0.78}\text{Gd}_{0.22}\text{O}_{1.89}$ , (CGO) thin films were prepared by an airblast spray pyrolysis technique (SP) and by pulsed laser deposition (PLD). The substrate material was in all cases a sapphire single crystal (Stettler, Switzerland) with a (11 $\bar{2}$ 0) surface orientation parallel to the substrate. In spray pyrolysis a precursor solution is atomized to very fine droplets by air pressure. Precursor droplets hitting the heated substrate undergo pyrolytic decomposition and produce an amorphous metal oxide thin film. The process is described in detail elsewhere [29]. For the CGO thin films a precursor solution of 0.1 mol/l was produced by dissolving 0.02 mol/l gadolinium chloride (Alfa Aesar, 99.9% purity) and 0.08 mol/l cerium nitrate (Alfa Aesar, 99.5% purity) in a solution of 33:33:33 vol% ethanol, diethylene glycol monobutyl ether and methoxy propanol (all solvents from Fluka Chemie, 99.0% purity). The precursor solution was fed to the spray gun with a liquid flow rate of 34.4 ml/h and atomized by the spray gun (Compact 2000KM, Böhler Verfahrenstechnik, Germany) with 1 bar air pressure. The droplets produced in this manner were sprayed on a heated sapphire single crystal situated on a hot plate (CERAN 500, type 11A, Germany) at a substrate temperature of  $310 \pm 10$  °C for 3 h. Before spray deposition, the sapphire substrate temperature was directly measured on the substrate by a contact thermocouple. For the undoped ceria thin films, all parameters were kept identical to the CGO films, except that no gadolinium salt was added to the precursor.

For comparison,  $\text{Ce}_{0.74}\text{Gd}_{0.26}\text{O}_{1.9-x}$  thin films ranging from 400 to 800 nm in thickness were also produced on sapphire by PLD (SURFACE, Hüchelhoven, Germany) using a KrF excimer laser with 248 nm wavelength. The PLD process was performed at room temperature at a pressure of  $10^{-3}$  mtorr, with 10 Hz laser pulse repetition

frequency, 200 mJ energy per pulse and at 45 mm target substrate distance. The targets were produced as follows:  $\text{Ce}_{0.8}\text{Gd}_{0.2}\text{O}_{1.9-x}$  powder (Praxair, purity 99.9%) was uniaxially and then isostatically pressed (850 kN for 3 min). The resulting pellets were heated up to 1400 °C with a rate of 3 °C/min, held at this temperature for 4 h and cooled down to room temperature at 5 °C/min. The densities of the obtained pellets measured by Archimede's method were >98% of the theoretical value.

Film thickness, microstructure and morphology were evaluated by scanning electron microscopy (Field emission SEM, LEO 1530, Germany). Chemical composition was determined by dispersive X-ray analysis spectroscopy (EDX, LEO 1530) and X-ray photoelectron spectroscopy (XPS, PHI Quantera SXM). The X-ray source of XPS was a monochromatic Al  $K\alpha$  (1486.6 eV) run at 25 W and 15 kV. Survey spectra were carried out at 280 eV pass energy and 1 eV step size. The crystallinity was investigated by X-ray diffraction (XRD, Bruker AXS D8 Advance). In addition, differential scanning calorimetry and thermogravimetry (DSC/TG, Netzsch STA 449 C) were performed. Outgassing species attributed to mass losses during TG, were detected by a mass spectrometer (M, Balzers Quadstar 422).

### 3.2. Grain growth study

#### 3.2.1. In situ XRD grain growth study for average grain sizes below 80 nm

For average grain sizes smaller than 80 nm the time and temperature dependence of grain growth was studied in situ during heat treatment by X-ray diffraction and evaluated using the Scherrer equation. The line widths of the Bragg peaks provide information on the average grain size and on defects of the crystal lattice originating from microstrain. Grain orientation effects can be deduced from the intensity ratio between the diffraction lines of different crystal lattice directions. For the XRD experiments, the samples were enclosed in a furnace (Anton Paar HTK 1200), which was integrated in the XRD set up. Diffracted X-rays from the sample were detected by a position sensitive detector (Braun PSD ASA-S) with which X-ray photons from 400 nm thick CGO thin films could be detected with higher resolutions and in shorter time intervals compared to conventional scintillation counters. The XRD set up was equipped with a copper radiation source ( $\lambda = 0.15404$  nm) at 40 kV and 40 mA followed by a  $K\alpha_1$ -Ge monochromator (Bruker AXS). For grain growth analysis the (111) and (200) peaks were used within the  $2\theta$ -range 26–32°. The  $2\theta$  interval was kept as small as possible to avoid perceptible microstructural changes during the recording of the XRD pattern. A heating and cooling rate of 3 °C/min was chosen for all experiments. Every 40 min an XRD pattern was recorded for isothermal dwell times between 1 and 30 h. This method allowed isothermal in situ grain growth studies. The average grain size was determined from the full width at half maximum (FWHM),

by using Fourier analysis of the XRD peaks, refined by a split Pearson 7 function (Software EVA 6.0), of the (111) peak. The FWHM results from peak broadening due to instrumental broadening,  $\text{FWHM}_i$ , and microstructure,  $\text{FWHM}_c$ . The instrumental peak broadening of the diffractometer was determined by measuring a commercially available microcrystalline and stress-free CGO powder. By the Warren and Biscoe equation the instrumental broadening  $\text{FWHM}_i$  can be eliminated from FWHM [30]:

$$\text{FWHM}_c^2 = \text{FWHM}^2 - \text{FWHM}_i^2 \quad (5)$$

Average grain size and microstrain were calculated from  $\text{FWHM}_c$  according to the Scherrer and Wilson equation [31,32]:

$$\text{FWHM}_c = \frac{4K\lambda}{3 \cos \theta \cdot G} + 4\varepsilon \cdot \tan \theta \quad (6)$$

Here, the Scherrer constant  $K$  equals 0.89 for spherical grains,  $\lambda$  denotes the X-ray wavelength,  $\theta$  the diffraction angle,  $G$  the average grain size and  $\varepsilon$  the microstrain. Applying the so-called Williamson-Hall technique [33] to Eq. (6), one plots the  $\text{FWHM}_c \cos \theta$  versus  $\sin \theta$  and determines the average grain size and microstrain, respectively, by extracting their value from the ordinate intersection ( $4K\lambda/3G$ ) and the slope ( $4\varepsilon$ ), respectively.

The lattice parameter of the cubic CGO crystal lattice was calculated from the position of the observed diffraction lines in the XRD pattern, according to the following relation:

$$a = \frac{\lambda \sqrt{(h^2 + k^2 + l^2)}}{2 \sin \theta} \quad (7)$$

In this equation  $a$  indicates the lattice parameter of the cubic crystal lattice and  $h$ ,  $k$  and  $l$  the Miller indices of the considered Bragg reflection.

#### 3.2.2. Ex situ SEM grain growth study for average grain sizes larger than 80 nm

Average grain sizes larger than 80 nm cannot be determined by XRD because of its limited instrumental resolution. Hence, grain growth of larger grain sizes was conducted by ex situ isothermal annealing of samples and subsequent SEM analysis. For this purpose CGO thin films were heated and cooled at 3 °C/min to the target temperature and isothermally held for times ranging from 1 to 30 h. The samples were air quenched after an isothermal hold and analyzed by SEM. The average grain size was determined by measuring up to 300 grain intercept lengths of three different spots on the CGO thin film. Conversion of intercept length to grain size was obtained by the multiplication with the grain size conversion factor 1.56.

## 4. Results and discussion

### 4.1. Thermal treatment of spray pyrolysis thin films

The chemistry of our spray pyrolysis thin films was analyzed as a function of temperature by DSC and TG

measurements whereby outgassing species were detected by mass-spectrometry during heating and cooling (Fig. 1). When thin films are deposited by spray pyrolysis the material is amorphous and crystallization occurs during the first annealing for temperatures above the film deposition temperature [29]. Amorphous thin films were scratched off from the substrate and the obtained powder (with an original mass of 126.24 mg) was heated in air from room temperature to 1200 °C at 10 °C/min. By DSC and mass-spectrometry a large endothermic signal with a peak maximum at 180 °C due to adsorbed water and a broad exothermic signal between 400 and 1000 °C due to carbon combustion were detected. The remaining carbon content in the thin films is from the alcoholic precursor used during the spray pyrolysis process. The total weight loss between room temperature and 1200 °C was 6.34% and it can be confirmed that it is mainly due to outgassing water and residual carbon.

In Fig. 2 the XRD pattern of a CGO spray pyrolysis film annealed at 800 °C is shown. The XRD pattern shows reflections of the cubic fluorite crystal structure type [34] with a lattice parameter of  $0.540 \pm 0.001$  nm for the CGO thin film, see Table 1. The XRD pattern shown here represent a well-crystallized material and the determined lattice parameter is in good agreement with the one from the literature [35–38].

In Fig. 3 the influence of the thermal treatments on the XRD peak shapes of the (111) and (200) reflections (Fig. 3a), the grain orientation along those reciprocal crystal directions (Fig. 3b), and the microstrain (Fig. 3c) are displayed.

In Fig. 3a it can be recognized that directly after thin film deposition broadened (111) and (200) peaks appear. Further temperature increase to 500 °C does not affect the broad peak shapes of (111) and (200) and it can be concluded that between room temperature and 500 °C a predominantly amorphous thin film is present. At temperatures above 500 °C sharpening of the Bragg peaks indi-

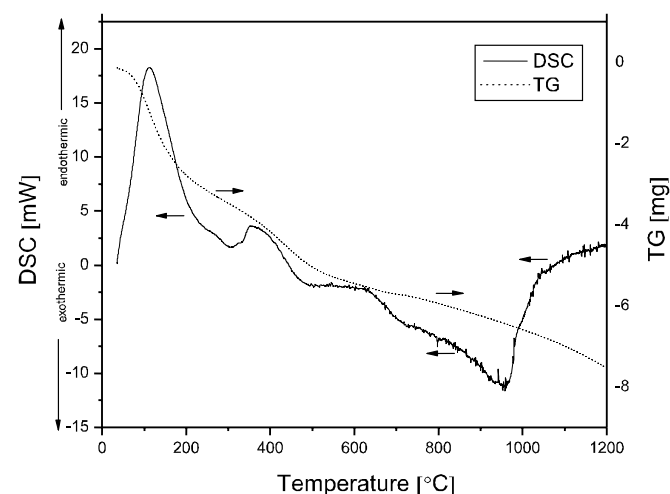


Fig. 1. DSC and TG of a CGO spray pyrolysis thin film.

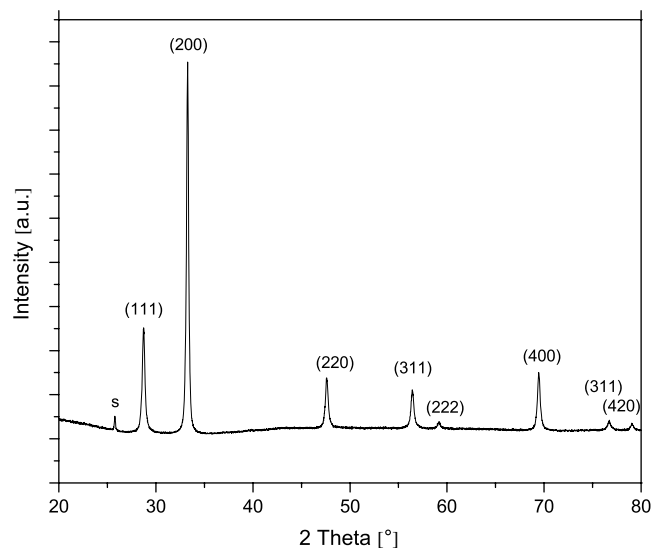


Fig. 2. XRD pattern of a CGO spray pyrolysis thin film on sapphire annealed at 800 °C. (The CGO peaks are designated by Miller indices and the sapphire peak is denoted by s).

cates crystallization of the films. At temperatures above 800 °C well-crystallized material is obtained.

The grain orientations as a function of temperature are shown in Fig. 3b. The peak intensity ratio  $I(111)/I(200)$  is mapped for various annealing temperatures. (The change of the grain orientations during thermal treatment is indicated by changes in the proportion of the different peak intensities.) For temperatures lower than 600 °C the (111) peak shows the highest peak intensity and the (200) the second highest ( $I(111)/I(200) > 1$ ). At higher temperatures the (200) peak dominates with respect to the (111) reflection ( $I(111)/I(200) < 1$ ) as the (200) peak intensity increases rapidly in contrast to the intensity of the (111) peak with temperature. Preferred (200) grain orientation perpendicular to the substrate develops during heating from room temperature to 1200 °C in as-deposited CGO thin films and texture develops. Similar grain orientations have already been observed for spin coated films on sapphire and chemical vapor deposited (CVD) CGO thin films on NiO-YSZ discs [11,39]. In those films  $I(111)/I(200) > 1$  was observed for low, and  $I(111)/I(200) < 1$  for high temperatures. However, the temperature where  $I(111)/I(200) = 1$  occurs in our films is roughly 550 °C, whereas the CVD film showed  $I(111)/I(200) = 1$  at 500 °C and the spin coated film at 1200 °C. As this

Table 1  
Lattice constants of CGO

Lattice constant (nm)	Average grain size (nm)	Sample preparation
0.540	20	Spray pyrolysis [this study]
0.542	65	Powder [35]
0.541–0.542	–	Sintered pellet [36]
0.541–0.542	1000–3000	Sintered pellet [37]

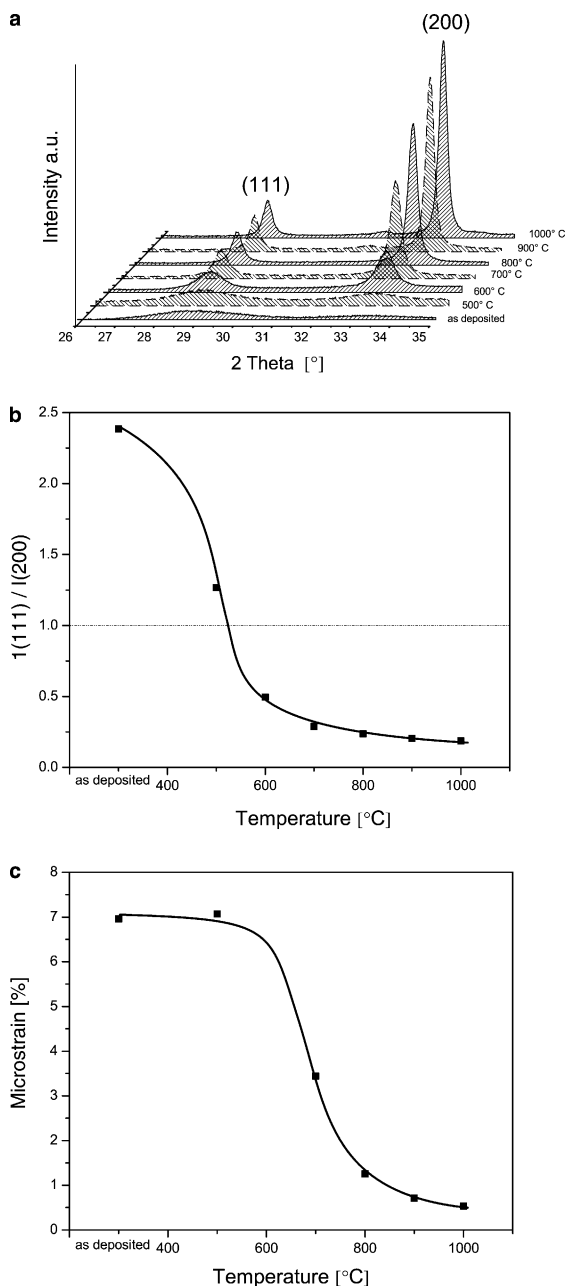


Fig. 3. (a) Thermal treatment of CGO spray pyrolysis thin films: crystallization, (b) grain orientation given by the peak intensity ratio  $I(111)/I(200)$  and (c) microstrain.

observation has been made on different substrates with different orientations, it is reasonable to assume that these texturing effects are not related to the substrate orientation.

Fig. 3c displays the influence of temperature on the microstrain within the CGO film. Between room temperature and 500 °C the microstrain remains unchanged, due to the amorphous nature of the films (see also Fig. 3a). With progressing thermal treatment (500–1000 °C) the microstrain decreases due to ordering of the atoms in the crystal lattice and the concentrations of stacking faults and point defects are reduced. Suzuki et al. observed a similar decrease of microstrain when crystallizing doped and

undoped (amorphous) spin coated ceria thin films [11,40]. At an average grain size of 20 nm Suzuki et al. report a microstrain as low as  $\sim 0.003\%$  for CGO. The films generated by spray pyrolysis in the present study exhibit a larger microstrain of 0.125% for the same average grain size. Therefore, a higher defect concentration appears to exist in our films.

Microstructures were also characterized by SEM. In Fig. 4 the microstructures of a CGO SP sample annealed at 1100 °C for 0 h are shown in top (Fig. 4a and b) and cross section views (Fig. 4c and d). It is evident that even at a temperature as high as 1100 °C and after air quenching, crack- and pore-free thin films are retained. The high magnification plane view of the CGO film of Fig. 4a shows dark and light shaded regions referring to thickness differences of the thin film. Those thickness differences result from the statistic distribution of droplets arriving onto the substrate during spray pyrolysis deposition. For the SP film thicknesses in the present study, local variations of  $\pm 40$  nm might be present. From the micrographs of the cross sections a film thickness of 400 nm was determined for 3 h deposition time. This corresponds to a thin film SP deposition rate of 130 nm/h. As the average grain sizes throughout all experiments were smaller than 250 nm, the kinetics of grain growth were not affected by the finite thickness of the film. The influence of different annealing temperatures from 1000 to 1200 °C without isothermal hold on the microstructure is shown in Fig. 5. The grains have globular shape and have not developed flat habitus planes on the film surfaces, even for the highest temperature. This is different from high-temperature isothermally annealed films (1100 and 1200 °C) in which flat habitus planes and finally faceting developed with prolonged dwell times.

The chemical compositions of the SP films were analyzed by EDX using the cerium and gadolinium *L*-lines. All CGO thin films showed  $22 \pm 2$  atom% of gadolinia (based on the sum of the cations) in the ceria lattice. No additional phases could be identified either by SEM, EDX, XPS or XRD. From the literature it is known that impurities like  $\text{SiO}_2$  can occur as grain boundary films in zirconia and ceria ceramics which influence grain growth kinetics [41]. However, with XPS analysis no silicon could be detected in the spray pyrolysis thin films either prior to or after the isothermal dwell experiments.

#### 4.2. Isothermal grain growth and microstrain analysis of spray pyrolysis thin films

The isothermal grain growth data from XRD (in situ) and SEM (ex situ) analysis of CGO SP thin films are shown in Fig. 6. The grain growth occurs mostly in the first 5–10 h of dwell for an average grain size below 140 nm and an isothermal dwell temperature below 1100 °C. Then suddenly grain growth slows down and stable microstructures establish at an apparent limited grain size below 140 nm. This self-limited grain growth can be described by a relaxation

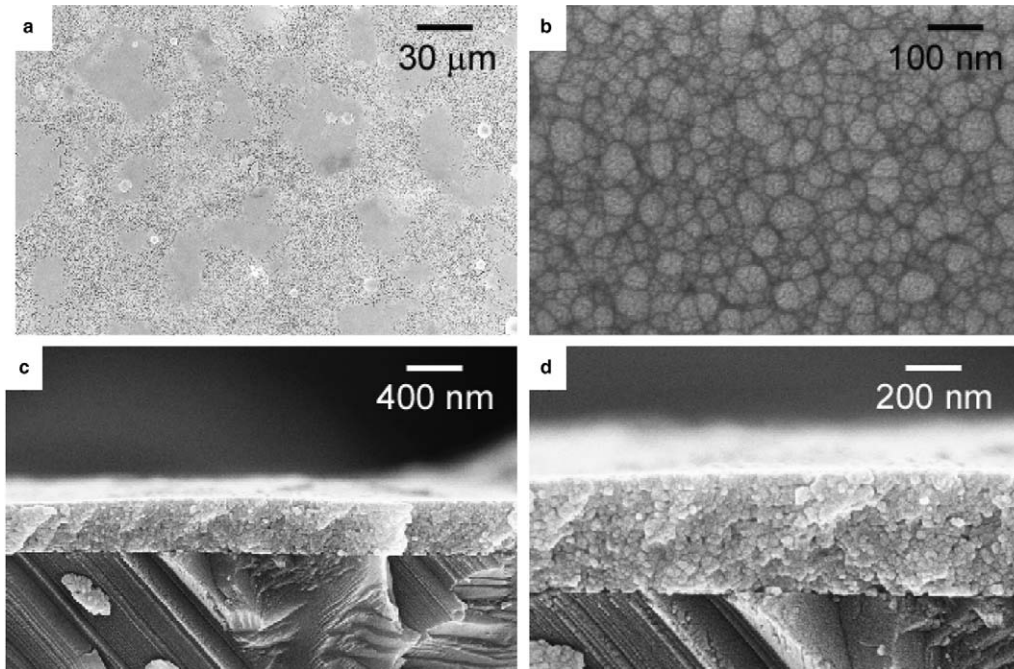


Fig. 4. Micrographs of the nanocrystalline CGO spray pyrolysis thin film on sapphire substrate annealed at 1100 °C: (a and b) top views and (c and d) cross sections at different magnifications.

function characterized by a relaxation time  $\tau_1$ , the limited grain size  $G_L$ , average grain size  $G$ , the initial grain size  $G_0$  and time  $t$ :

$$G - G_0 = (G_L - G_0) \left( 1 - \exp^{-\frac{t}{\tau_1}} \right) \quad (8)$$

In samples with grain sizes larger than 140 nm and for dwell temperatures higher than 1100 °C the grains continue to grow and common grain growth according to the gener-

alized grain growth Eq. (3) is observed. For the isothermal hold at 1200 °C a grain growth exponent of 7 with a correlation coefficient of 0.98 was determined.

The grain size distributions of CGO samples were followed for isothermal dwells from 1000 to 1200 °C. Results for 1100 °C are shown in Fig. 7. The frequencies of the grain sizes were plotted versus the normalized grain sizes. The size distributions are invariant with dwell time and

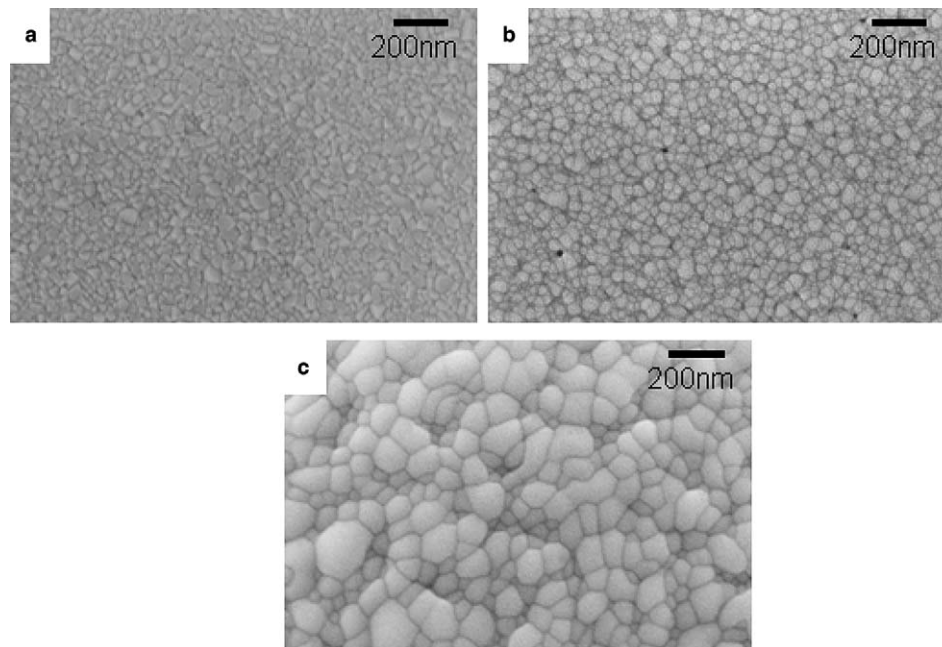


Fig. 5. Nanocrystalline CGO spray pyrolysis thin films on sapphire substrate as a function of temperature without an isothermal hold: (a) 1000 °C, (b) 1100 °C and (c) 1200 °C.

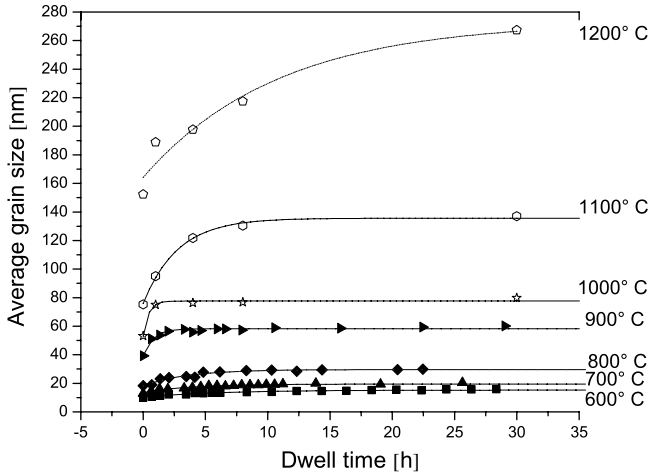


Fig. 6. Average grain size of the CGO spray pyrolysis films as a function of dwell time and temperature. Full symbols represent grain growth data determined by in situ measured by XRD technique and open symbols those from ex situ SEM analysis.

fulfill a log normal distribution with correlation coefficients in excess of 0.98. An example of the microstructures that develop during annealing at 1100 °C is shown in Fig. 8. The grains increase from 75 to 132 nm before 10 h dwell time and cease to grow further. For 0 and 1 h dwell times the grains show globular surfaces whereas flat and faceted grain faces developed after 4 and 30 h. An average number of grain faces in the plane 2D views from all examples of Fig. 8 of  $5.7 \pm 0.6$  was obtained (6.5 for 0 h, 5.1 for 1 h, 5.24 for 4 h and 6.24 for 30 h). No significant changes of the coordination number of grains could be detected in this time span. The SEM microstructures for the isothermal dwell at 1000 and 1200 °C were also analyzed. For an isothermal dwell at 1000 °C faceting of the grains with increasing dwell time could not be deduced. However, at 1200 °C faceting of the grains can already be observed after 1 h of dwell, leading to the conclusion that the grain faceting is thermally activated, but is in no relation to the limited grain growth.

The grain size distribution studies and SEM observations as a function of dwell time showed that no abnormal grain growth occurred during self-limited grain growth. It can also be concluded that faceting is not the cause for the self-limited grain growth, as it can only be observed at 1200 °C after short dwell times and at 1100 °C after long dwell times, but not at lower temperatures where the self-limited grain growth predominates.

In Fig. 9 the evolution of microstrain is analyzed as a function of temperature and dwell time and compared to the self-limited grain growth data. The microstrain decreases within the first 10 h of isothermal hold and is characterized by a relaxation time  $\tau_2$  and a residual microstrain  $\varepsilon_L$ . Latter signifies the reached microstrain after the relaxation. For the description of microstrain  $\varepsilon$  over time an exponential decay function was chosen:

$$\varepsilon = \varepsilon_L + \varepsilon_0 \exp^{-\frac{t}{\tau_2}} \quad (9)$$

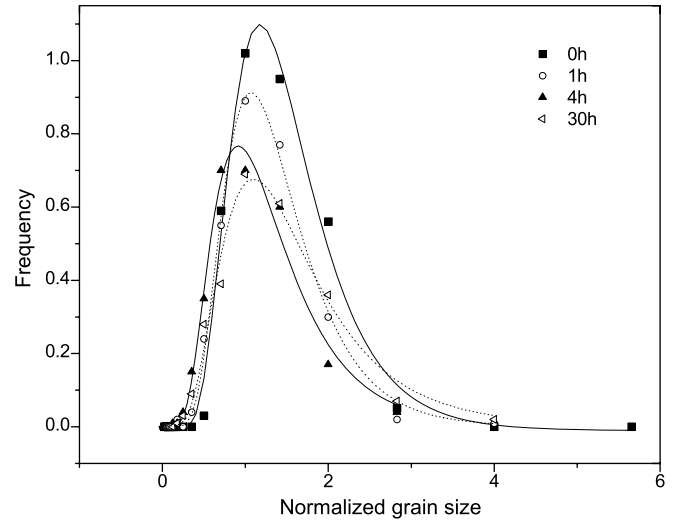


Fig. 7. Log normal grain size distributions in CGO spray pyrolysis thin films for isothermal hold at 1100 °C revealed from SEM micrographs.

Both the grain growth and the microstrain are for temperatures below 1100 °C and grains smaller 140 nm characterized by relaxation times and limited grain size  $G_L$  or residual microstrain  $\varepsilon_L$ . In Fig. 10 the relaxation times of the grain growth and the microstrain are summarized. Increasing temperature within the self-limited grain growth regime leads to a decrease of the relaxation times for grain growth as well as for microstrain. Microstrain and grain growth show relaxation times in the same order of magnitude and the kinetics are obviously temperature dependent.

The diffusion coefficients  $D_i$  have been determined as a function of annealing temperature according to [27]:

$$D_i = \frac{(G_L - G_0)^2}{4\tau_1} \propto \left( -\frac{Q}{k_B T} \right) \quad (10)$$

where  $G_L$  is the limited grain size,  $G_0$  is the starting grain size,  $\tau_1$  is the relaxation time of the self-limited grain growth (see Eq. (8)),  $Q$  the activation energy,  $k_B$  the Boltzmann constant and  $T$  the temperature. From Fig. 11 an activation energy of  $1.32 \pm 0.1$  eV with a correlation coefficient of 0.98 was calculated for the diffusion coefficient. Activation energies between 6.6 and 9.6 eV have so far been determined for the contribution of grain boundary and volume diffusion in micrometer grained CGO [13,42]. For the low activation energy of 1.32 eV in the present study mainly grain boundary diffusion can be assumed to contribute in the grain coarsening. So far, volume diffusion seems not to contribute to the self-limited grain growth of the nanocrystalline CGO thin films.

We observe at low temperature ( $\leq 1100$  °C) self-limited grain growth and the relaxation of the microstrain after a relaxation time. When the temperatures are above 1100 °C the microstrain of the thin films fully relax and the temperature is sufficiently high to activate volume diffusion in addition to the grain boundary diffusion and common grain growth kinetics (see Eq. (3)) dominate.

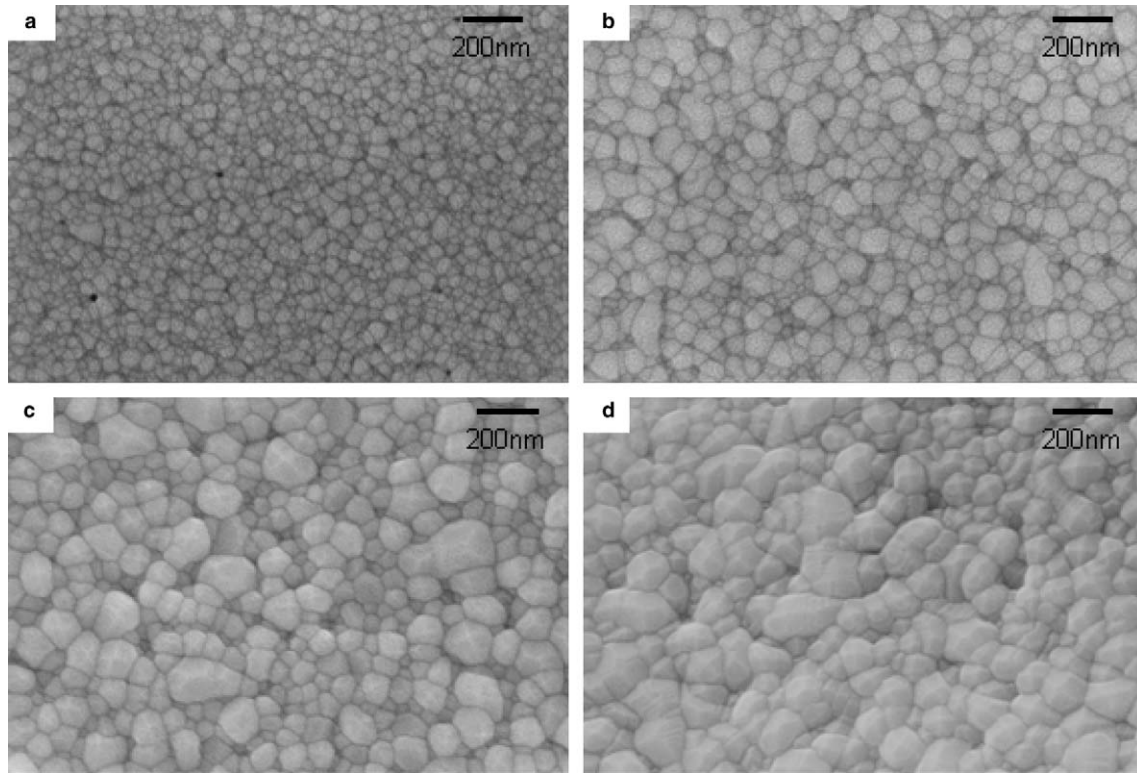


Fig. 8. Micrographs of nanocrystalline spray pyrolysis CGO thin films on sapphire substrate for different dwell times at 1100 °C: (a) 0 h, (b) 1 h, (c) 4 h and (d) 30 h.

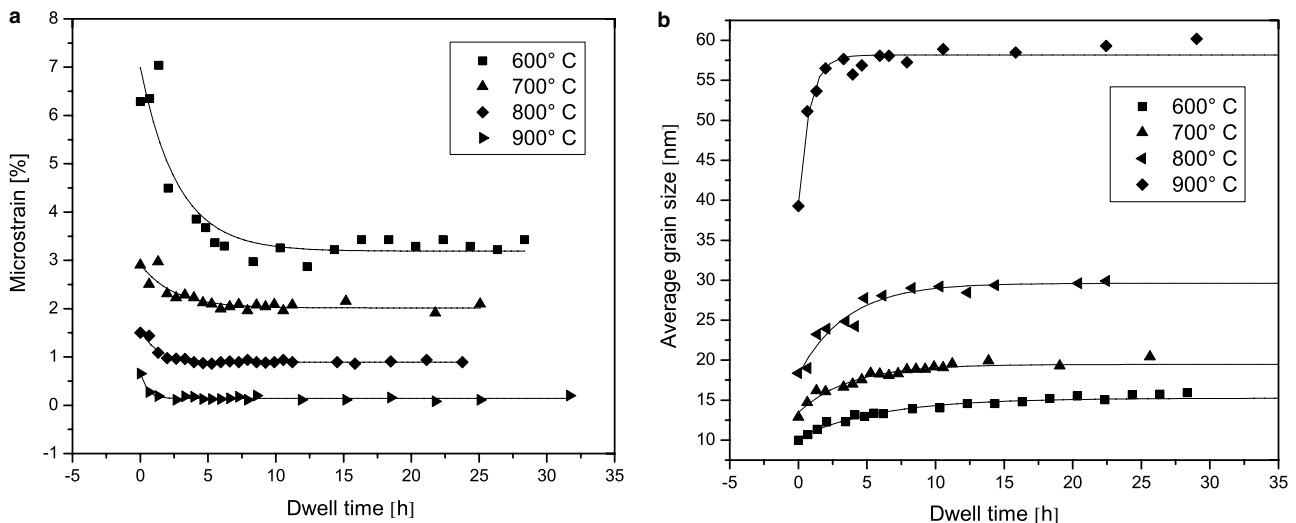


Fig. 9. Grain growth and microstrain of the CGO spray pyrolysis films as a function of dwell time and temperature as determined from in situ XRD measurements.

#### 4.3. Influence of the preparation method on self-limited grain growth of CGO thin films

The influence of spray pyrolysis related impurities, i.e., carbon residues present up to 1000 °C (Fig. 1) on the observed self-limited grain growth was investigated by a study of the grain growth kinetics in PLD prepared CGO thin films. The PLD thin films preparation is com-

pletely different compared to spray pyrolysis as no organic precursors are involved and the starting material is a sintered ceramic pellet. The dense PLD films had a thickness of 800 nm. After deposition of the PLD films the initial average grain size was 15 nm and the chemical composition of  $\text{Ce}_{0.74}\text{Gd}_{0.26}\text{O}_{1.9-x}$  was confirmed by EDX analysis. Annealed CGO films prepared by PLD were analyzed by XPS at the surface and after etching roughly

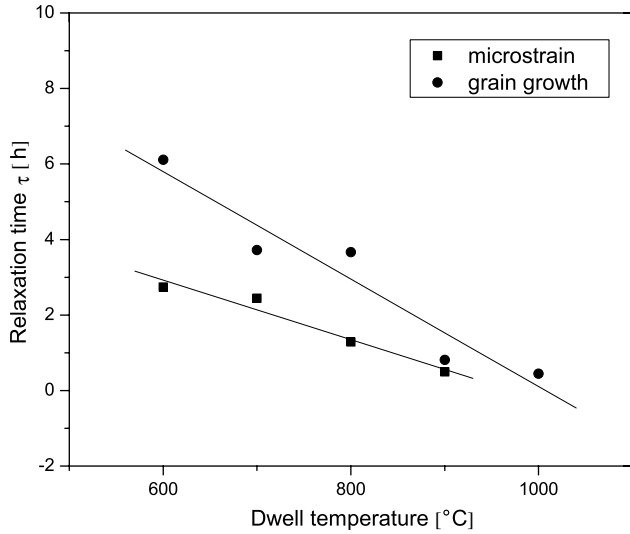


Fig. 10. Microstrain and grain growth relaxation time as a function of dwell temperature for CGO spray pyrolysis thin films.

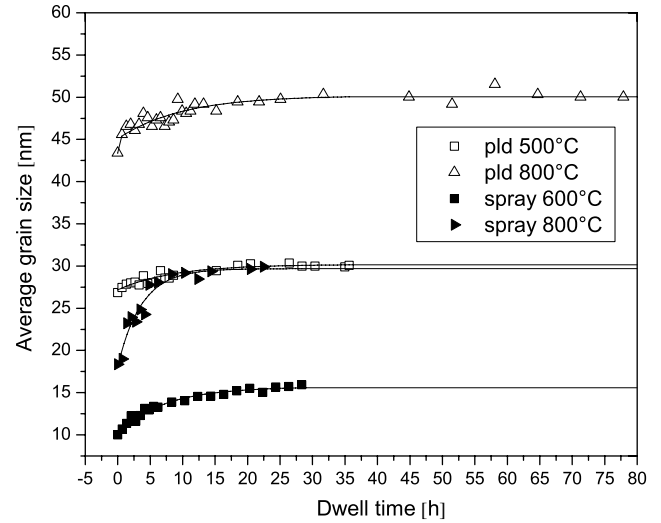


Fig. 12. Comparison of the grain size versus dwell time of spray pyrolysis and PLD prepared CGO thin films.

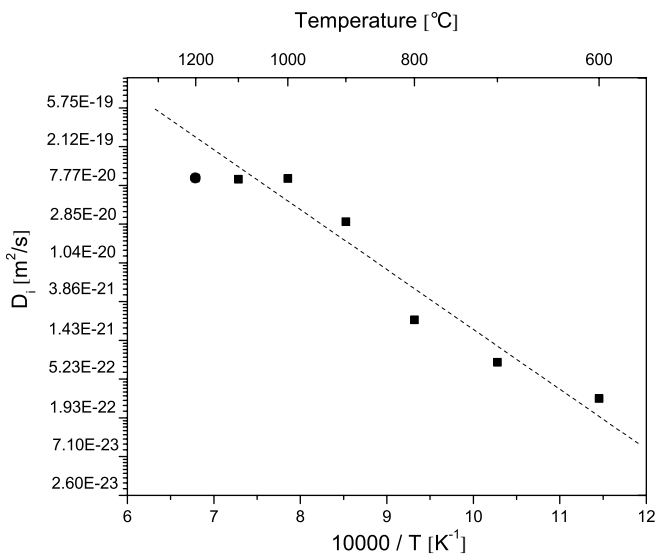


Fig. 11. Diffusion coefficient  $D_i$  as a function of temperature for CGO spray pyrolysis thin films.

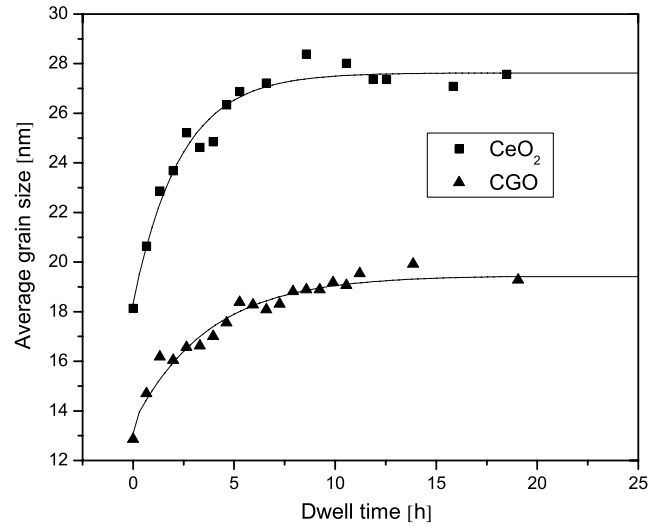


Fig. 13. Grain growth of doped and undoped ceria for isothermal dwell at 700 °C. Thin film preparation method was in both cases spray pyrolysis.

90 nm of the film thickness away. Neither silicon nor other impurities could be detected. The grain growth of the PLD thin film was studied by in situ XRD and the grain size is shown in Fig. 12. At dwell temperatures of 500 and 800 °C grain growth occurred during the first 15 h of dwell, then grain growth ceased. Once a metastable microstructure has established no further grain growth was observed for over 60 h, as demonstrated for the case of the 800 °C sample.

These results demonstrate clearly that the self-limited grain growth occurs at low annealing temperatures independent on the CGO thin film preparation method, which means independently of residual carbon impurities that are inevitably present up to 900 °C in the SP films.

#### 4.4. Influence of gadolinia doping in ceria on self-limited grain growth

The influence of the gadolinia doping on grain growth is demonstrated in Fig. 13. Here, a comparison of the grain growth of undoped  $\text{CeO}_2$  and CGO ( $\text{Ce}_{0.78}\text{Gd}_{0.22}\text{O}_{1.89}$ ) is shown. Both films were prepared by the SP method and crystallized upon heating (at 3 °C/min) to 700 °C, where the films were isothermally held. The undoped material already shows an average grain size of 18 nm after crystallization whereby the ceria solid solution shows a smaller grain size of 12.5 nm. As expected from solute drag theory [43] grains grow faster in the undoped material compared to grains of the solid solution. Similar to the CGO the undoped ceria shows stable microstructures after 10 h isothermal annealing reaching a limited grain size of 27 nm.

The gadolinia doping in ceria retards grain growth due to solute drag. However, self-limited grain growth is observed in doped as well as in undoped spray pyrolysis thin films and is not caused by the trivalent doping.

## 5. Summary and conclusion

Amorphous, dense and crack free undoped and gadolinia-doped ceria thin films were deposited by spray pyrolysis and PLD on sapphire single crystal substrates. Dense amorphous (SP) and nanocrystalline films were obtained. Isothermal grain growth studies show that the grains grow within the first 5–10 h of dwell for temperatures below 1100 °C and average grain sizes below 140 nm until metastable microstructures with limited grain sizes are established. At higher annealing temperatures common curvature-driven grain growth is observed.

At low temperatures (<1100 °C) the thin films are in a metastable state characterized by self-limited grain growth and the microstrain relaxation. The grain growth in this metastable state is characterized by grain boundary diffusion. At higher temperatures (>1100 °C) the microstrain has fully relaxed and the material is well-crystallized. Then common grain coarsening and grain growth kinetics like in microcrystalline ceramics can be observed. From the correlation between self-limited grain growth and microstrain relaxation it can be concluded that PLD films deposited at room temperature under vacuum contain less microstrain than SP films deposited at 310 °C.

The self-limited grain growth in these nanocrystalline ceramics for temperatures <1100 °C is not dependent on the thin film processing method. Grain coarsening in pure CeO<sub>2</sub> shows accelerated kinetics compared to solid solutions (CGO) as expected from the influence of solute drag by the gadolinia dopant.

CGO thin films prepared by spray pyrolysis and PLD with grain sizes below 140 nm are surprisingly resistant towards thermally activated microstructural coarsening and are therefore promising electrolytes for operating temperatures below 800 °C and might be useful for  $\mu$ -SOFC applications.

## Acknowledgments

We thank Dr. Wörle and Prof. Nesper from the Inorganic Solid State Chemistry laboratory of ETH Zurich (Switzerland) for the use of the X-ray diffraction, the colleagues of the Laboratory of Surface Science and Technology of ETH Zurich (Switzerland) for XPS analysis, and Dr. Eva Jud for helpful discussion.

The project was supported by the Swiss Federal Office of Energy, Project Number 100430.

## References

- [1] Kleinlogel C, Gauckler LJ. *Solid State Ionics* 2000;135:567.
- [2] Skinner SJ, Kilner JA. *Mater Today* 2003;6:30.
- [3] Steele BCH. *J Power Sources* 1994;49:1.
- [4] Ormerod RM. *Chem Soc Rev* 2002;32:17.
- [5] Perednis D, Gauckler LJ. *Solid State Ionics* 2004;166:229.
- [6] Will J, Mitterdorfer A, Kleinlogel C, Perednis D, Gauckler LJ. *Solid State Ionics* 2000;131:79.
- [7] Tompsett GA, Finnerty C, Kendall K, Alston T, Sammes NM. *J Power Sources* 2000;86:376.
- [8] Gödickemeier M, Gauckler LJ. *J Electrochem Soc* 1998;145:414.
- [9] Kleinlogel C. PhD, ETH Zurich Nr. 13483 1999.
- [10] Choy K, Bai W, Charojrochkul S, Steele BCH. *J Power Sources* 1998;71:361.
- [11] Suzuki T, Kosacki I, Anderson HU. *Solid State Ionics* 2002;151:111.
- [12] Taniguchi I, van Landschoot RC, Schoonman J. *Solid State Ionics* 2003;160:271.
- [13] Jud E, Huwiler CB, Gauckler LJ. *J Am Ceram Soc* (submitted for publication).
- [14] Burke JE. *Trans Am Inst Mining Metall Eng* 1949;180:73.
- [15] Burke JE, Turnbull E. *Prog Metal Phys* 1952;3:220.
- [16] Atkinson HV. *Acta Metall* 1988;36:469.
- [17] Yan MF, Cannon RM, Bowen HK. Grain boundary migration in ceramics. In: Richard M, Fulrath RM, Pask JA, editors. *Ceramic microstructures '76*. Boulder, Colorado: Westview Press; 1976.
- [18] Zhang TS, Ma J, Kong LB, Zeng ZQ, Hing P, Kilner JA. *Mater Sci Eng B* 2003;103:177.
- [19] Zhang T, Hing P, Huang H, Kilner J. *Mater Lett* 2002;57:507.
- [20] Malow TR, Koch CC. *Acta Mater* 1997;45:2177.
- [21] Ganapathi SK, Owen DM, Chokshi AH. *Scripta Metall Mater* 1991;25:2699.
- [22] Sagel-Ransijn CD, Winnubst AJA, Burggraaf AJ, Verweij H. *J Eur Ceram Soc* 1997;17:1133.
- [23] Natter H, Schmelzer M, Löffler MS, Krill CE, Fitch A, Hempelmann R. *J Phys Chem B* 2000;104:2467.
- [24] Moelle CH, Fecht HJ. *Nanostruct Mater* 1995;6:421.
- [25] Natter H, Löffler M-S, Krill CE, Hempelmann R. *Scripta Mater* 2001;44:2321.
- [26] Schell N, Jensen T, Petersen JH, Andreasen KP, Bottiger J, Chevallier J. *Thin Solid Films* 2003;441:96.
- [27] Löffler JF, Johnson WL. *Appl Phys Lett* 2000;76:3394.
- [28] Löffler JF, Bossuyt S, Glade SC, Johnson WL, Wagner W, Thiyagarajan P. *Appl Phys Lett* 2000;77:525.
- [29] Perednis D, Wilhelm O, Pratsinis SE, Gauckler LJ. *Thin Solid Films* 2005;474:84.
- [30] Wagner CNJ, Aqua EN. *J Less Common Metals* 1965;8:51.
- [31] Scherrer P. *Nachrichten von der Königlichen Gesellschaft der Wissenschaft zu Göttingen, Mathematisch-physikalische Klasse*. 1918;1:98.
- [32] Wilson AJC. *X-ray. Optics* 1949;5.
- [33] Hall W, Williamson GK. *Acta Metall* 1953;1:22.
- [34] Zhang TS, Ma J, Kong LB, Hing P, Kilner JA. *Solid State Ionics* 2004;167:191.
- [35] Dikmen S, Shuk P, Greenblatt M, Gomez H. *Solid State Sci* 2002;4:585.
- [36] Lewis GS, Atkinson A, Steele BCH, Drennan J. *Solid State Ionics* 2002;152–153:567.
- [37] Ma J, Zhang TS, Kong LB, Hing P, Chan SH. *J Power Sources* 2004;132:71.
- [38] Zhang TS, Ma J, Kong LB, Chan SH, Hing P, Kilner JA. *Solid State Ionics* 2004;167:203.
- [39] Song HZ, Wang HB, Zha SW, Peng DK, Meng GY. *Solid State Ionics* 2003;156:249.
- [40] Suzuki T, Kosacki I, Anderson HU, Colomban P. *J Am Ceram Soc* 2001;84:2007.
- [41] Allemann JA, Michel B, Marki H-B, Gauckler LJ, Moser EM. *J Eur Ceram Soc* 1995;15:951.
- [42] Lewis GS. PhD, Department of Materials, Imperial College of Science, Technology and Medicine, London 2002.
- [43] Cahn JW. *Acta Metall* 1962;10:798.